Title	Removal of Hydrogen Sulfide and Ammonia by Goethite-Rich Limonite in the Coexistence of Coke Oven Gas Components
Author(s)	Mochizuki, Yuuki; Ogawa, Ayumu; Tsubouchi, Naoto
Citation	ISIJ International, 57(3), 435-442 https://doi.org/10.2355/isijinternational.ISIJINT-2016-561
Issue Date	2017-03-15
Doc URL	http://hdl.handle.net/2115/79332
Rights	
Type	article
File Information	ISIJ Int. 57(3)_ 435-442 (2017).pdf

Instructions for use

Removal of Hydrogen Sulfide and Ammonia by Goethite-Rich Limonite in the Coexistence of Coke Oven Gas Components

Yuuki MOCHIZUKI, Ayumu OGAWA and Naoto TSUBOUCHI*

Center for Advanced Research of Energy and Materials, Faculty of Engineering, Hokkaido University, Kita 13 Nishi 5, Kita-ku, Sapporo, Hokkaido, 060-8628 Japan.

Hydrogen sulfide (H_2S) removal and catalytic ammonia (NH_3) decomposition performance of limonite in the presence of coke oven gas (COG) components has been studied in a cylindrical quartz reactor at 300–850°C under a high space velocity of 51 000 h^{-1} to develop a novel hot gas cleanup method. The H_2S removal behavior in 50% H_2/He depends on the temperature, with high performance observed at lower temperature. An investigation of the removal behavior of H_2S in the presence of COG components (CH_4, CO, CO_2 and H_2O) at 400°C reveals that CH_4 does not affect the removal performance. On the other hand, the coexistence of CO drastically decreases the H_2S removal performance. However, the addition of 5% H_2O to 50% H_2/30% CH_4/5% CO/He dramatically improves the H_2S removal performance, whereas the performance is low at 5% CO_2 with 50% H_2/30% CH_4/5% CO/He. In addition, the H_2S breakthrough curve strongly depends on the space velocity.

The limonite catalyst achieves almost complete decomposition of NH_3 in He at 850°C until 240 min. When the decomposition run is performed in the presence of COG components, the coexistence of 30% CH_4 deactivates limonite with significant formation of deposited carbon. On the other hand, the addition of 5% CO_2, 5% H_2O or 5% CO_2/5% H_2O to 50% H_2/30% CH_4/5% CO improves the catalytic activity without carbon deposition, and >99% conversion of NH_3 to N_2 is maintained until 240 min.

KEY WORDS: hydrogen sulfide; ammonia; removal; decomposition; catalyst; limonite; coke oven gas.

1. Introduction

Coke oven gas (COG) produced during coal carbonization is generally used as a fuel source for coke ovens and other combustion units in iron steel making process. COG has recently attracted much attention as a low-cost source of hydrogen and value-added products for the chemical industry.[1] However, COG contains a variety of impurities, such as hydrogen sulfide (H_2S) and ammonia (NH_3), which are detrimental in some industrial applications. In conventional processes, the hot raw COG (>800°C) must be quenched to near room temperature using aqueous ammonia solution to remove tarry materials contained in the COG.[1] On the other hand, the catalytic or noncatalytic reforming of COG is a promising technology that effectively utilizes the energy of the hot COG.[2–5] Upon coal carbonization, some of the nitrogen and sulfur present in coal are retained in the solid phase, and the rest is released as volatile-N (N_2, NH_3, HCN and tar-N) and -S (H_2S, COS, CS_2 and tar-S) species.[6] It is well known that NH_3, HCN, tar-N, H_2S, organic-S and tar-S not only serve as sources of NO_x and SO_x but also are catalyst poison materials used for COG reforming and/or gas tube corrosion.

Our research group has been working on vapor deposition of gaseous-tar, which is contained in COG, into the pores of limonite or cold-bonded pellets to develop carbon-containing iron materials (composite) with enhanced strength and reducibility for blast furnaces.[7] A vapor deposition temperature of 350°C is optimum for obtaining completely filled mesopores in limonite or cold-bonded pellets using carbonaceous materials derived from tar via vapor infiltration. However, during vapor deposition treatment, N and S in the feed gases are likely to transfer from the gas-phase to the composite, which may cause high N and S contents in the resulting composite. When such a composite is used for blast furnaces, the N and S species in the composite may have adverse effects on the reduction rate, strength or exhaust gas purification equipment. N and S in COG mainly exist as NH_3 and H_2S, with contents of approximately 1 vol% and 3 000 ppmv, respectively. Therefore, it is very important to develop a removal method for gaseous-N and -S species in COG.

Our research group has been investigating the catalytic decomposition of NH_3 or model tar-N compounds (pyridine or pyrrole) using inexpensive iron catalysts.[8–18] We have found that fine particles of metallic iron (α-Fe) formed from low-value iron ore (limonite) give high activity in the decomposition of NH_3 and model tar-N compounds. Limonite can achieve almost complete decomposition of 2 000 ppmv NH_3 in inert or simulated fuel gas from coal gasification at 500–850°C.[10] In addition, we have recently

shown that the limonite-derived α-Fe can provide stable activity for the decomposition of 100 ppmv C_5H_5N to N_2 in He, with fuel gas or COG components at 500–850°C.[17,18] On the other hand, iron oxide is known to be effective for the removal of H_2S in fuel gas at 300–700°C.[19–23] Thus, it is possible that limonite-derived α-Fe will be a good adsorbent for H_2S in COG. However, only a few studies have reported H_2S removal in COG by iron-based adsorbents, such as iron oxide and/or iron-bearing sorbents combined with other metals.[24–27] It is well-known that a typical COG is composed of 54–59% H_2, 24–28% CH_4, 4–7% CO, 3–5% CO_2, 1–3% CO_2 and 1–3% H_2O with impurities, but the influence of the individual COG components on H_2S removal has not been investigated in previous reports.[24–27]

In this paper, therefore, we focus on investigating H_2S removal and catalytic NH_3 decomposition performance using an Australian limonite in the presence of COG components to develop a novel gas cleaning method for removing H_2S and NH_3.

2. Experimental

2.1. Sample

An Australian natural limonite ore composed of about 70% goethite (α-FeOOH) was employed in the present study. The metal composition of the limonite was Fe, 44; Si, 9.4; Al, 7.2; Mg, 0.15; and Ca, 0.07 mass%-dry.[17] The as-received limonite was sieved to select the 250–500 μm size fractions, and the Brunauer-Emmett-Teller (BET) specific surface area was measured as 40 m^2/g.

2.2. Hydrogen Sulfide Removal and Ammonia Decomposition

The experiments to evaluate H_2S removal and catalytic NH_3 decomposition performance were carried out in a cylindrical fixed-bed quartz reactor (8 mm i.d.) under ambient pressure. The details of the experimental apparatus have been described elsewhere.[17] The temperature was controlled with a K-type thermocouple attached to the exterior surface of the reactor. Approximately 0.25 g of limonite was first charged into the reactor with quartz wool, and a flow of high-purity He (>99.99995%) was then passed through the reactor until the concentration of N_2 in the experimental system decreased to less than 20 ppmv. After taking precautions against leakage, the reactor was heated electrically to 500°C. At this temperature, the He was replaced with high-purity H_2 (>99.9999%), and limonite was reduced by H_2 for 2 h. After the reduction pretreatment, the atmosphere was restored to He, and the reactor was held at a temperature of 300–850°C. The H_2S removal or NH_3 decomposition experiments began by passing 3 000 ppmv H_2S or 1 vol% NH_3 diluted with He and simulated COG (50% H_2/He, 50% H_2/30% CH_4/He, 50% H_2/30% CH_4/5% CO/He, 50% H_2/30% CH_4/5% CO/5% CO_2/He, 50% H_2/30% CH_4/5% CO/5% H_2O/He or 50% H_2/30% CH_4/5% CO/5% CO_2/5% H_2O/He) over the catalyst bed. The space velocity (SV) was maintained at 51 000 h^{-1} throughout each run, unless otherwise noted.

2.3. Gas Analysis

In the H_2S removal experiments, the H_2S concentration in the exit gas was measured using a standard detector tube (Gastec) at arbitrary times to obtain the breakthrough curves. The breakthrough and saturation points were defined as $C_i/C_0 = 0.1$ and 0.9, respectively. Here, C_0 and C_i are the initial concentration and the H_2S concentration in the exit gas at arbitrary time, respectively. The extent of sulfidation was calculated based on the iron content in limonite and the results of the breakthrough curves.

In the NH_3 decomposition runs, the amount of N_2 produced during the decomposition of NH_3 was measured at 3 min intervals with a high-speed micro gas chromatograph (GC; Agilent) equipped with a thermal conductivity detector. The conversion of NH_3 to N_2 was calculated based on the amount of NH_3 inlet and the N_2 concentration at the reactor exit.

2.4. Characterization

Powder X-ray diffraction (XRD; Shimadzu) measurements of the samples (as-received, after H_2 reduction and after H_2S removal or NH_3 decomposition) were performed with Mn-filtered Fe-Kα radiation. To avoid rapid oxidation of the α-Fe particles upon exposure to laboratory air, the limonite after H_2 reduction, H_2S removal or NH_3 decomposition was passivated using 1% O_2/He at room temperature and then recovered from the reactor.[10]

Temperature-programmed oxidation (TPO) was carried to quantitate the formation amounts of Fe_3C and C deposition during H_2S removal or NH_3 decomposition runs. In a TPO run, the limonite in the reactor after H_2S removal or NH_3 decomposition was first quenched to room temperature in a stream of high purity He and then heated at 10°C/min to 950°C in 10% O_2/He. The concentrations of CO and CO_2 evolved in this process were monitored using the micro GC. Some samples after TPO were also subjected to XRD measurements.

3. Results and Discussion

3.1. Effect of COG Components on H_2S Removal

This section focuses on the effect of coexisting of H_2, CH_4, CO, CO_2 and H_2O on H_2S removal by reduced-limonite. The changes in the breakthrough curves of reduced-limonite with temperature in 50% H_2/He were first examined, and the results are summarized in **Table 1**. In addition, the relationship between the extent of sulfidation and H_2S concentration in the exit gas based on the breakthrough curves are presented in **Fig. 1**. In the H_2S breakthrough curve at 300°C, a removal extent of 100% was measured until about 30 min, and the H_2S concentration in the exit gas increased after the breakthrough point at 40 min with increasing time on stream. The saturation point was observed at 65 min. Although similar tendencies were measured at 400, 500 and 600°C, the breakthrough points decreased with increasing temperature and were observed at 35, 30 and 24 min, respectively. On the other hand, at 700°C, the removal extent of H_2S decreased to 85% at 1 min after the experimental run start, and this value was maintained until 15 min. Subsequently, the H_2S removal extent decreased slightly to 75% until to 40 min, and then decreased with increasing time on stream, reaching saturation at 80 min. Although a similar tendency was observed at 800°C, the removal extent

of H_2S at 2 min after the experimental run start was 67%, which was smaller than that of 700°C. The above-mentioned breakthrough points corresponded to sulfidation extents of 0.75, 0.65, 0.55 and 0.45 at 300, 400, 500 and 600°C, respectively, as seen in Fig. 1, and these values decreased with increasing temperature. At 700 and 800°C (Fig. 1(b)), the reduced-limonite attained breakthrough points immediately after the runs started. These results suggest that H_2S removal by reduced-limonite in a reduction atmosphere (50% H_2/He) depends on the temperature and has higher efficiency at lower temperatures.

XRD measurements of limonite after the H_2S removal

Table 1. Summaries of breakthrough and saturation point at breakthrough curves , the extent of sulfidation and crystalline forms of Fe before and after H_2S removal in 50%H_2/He.

Temperature (°C)	Breakthrough point (min)	Saturation point (min)	Extent of Sulfidation $(H_2S/Fe)^a$	Iron species after H_2S removal^b
Reduced limonite	–	–	–	α-Fe
300	40	65	1.04	$Fe_{1-x}S$(m)
400	35	60	0.95	$Fe_{1-x}S$(m)
500	30	60	0.94	$Fe_{1-x}S$(m), FeS(w)
600	24	58	0.92	$Fe_{1-x}S$(m), FeS(m)
700	<1	80	0.93	$Fe_{1-x}S$(w), FeS(s)
800	<1	90	0.90	FeS(s)

^{a}After reaction. ^{b}XRD intensities designated by w (weak), m (medium), and s (strong).

runs were carried out to clarify the temperature dependencies of H_2S removal in 50% H_2/He. Table 1 also summarizes the results of the XRD measurements. The main peak attributed to $Fe_{1-x}S$ at approximately 55.8° was observed for the samples obtained after runs in 50% H_2/He at 300–400°C. On the other hand, the intensity of this peak gradually decreased with temperature (300–600°C), whereas the main peak at 600–800°C was observed at approximately 55.15°. This peak is attributed to FeS, and this observation indicates that the form of adsorbed H_2S on α-Fe changes with temperature. The H_2S/Fe ratios at after reaction in 50% H_2/He ranged from 0.9 to 1.05 (Table 1), and these values trended to decrease with increasing temperature. This result shows that almost all Fe in limonite was sulfidized by H_2S, and the difference in removal performance with increasing temperature is due to different adsorption forms ($Fe_{1-x}S$ and FeS). The sulfidation extent of more than 1.0 at 300°C in Fig. 1 and Table 1 is due to analytical error. As mentioned in the Introduction, the optimum vapor deposition conditions for preparing the composites, in which the carbonaceous material fills the mesopores in de-hydrated limonite via vapor deposition of gaseous-tar, is 350°C. Therefore, 400°C was used for H_2S removal by reduced-limonite in subsequently investigations.

Figure 2 shows the influence of coexisting gases on the relationships between the extent of sulfidation and H_2S concentration in the exit gas calculated from the H_2S breakthrough curves measured at 400°C in different feed gas compositions. The breakthrough and saturation points of the H_2S breakthrough curves and the extent of sulfidation at these points are summarized in **Table 2**. The breakthrough and saturation points in 50% H_2/He were observed at sul-
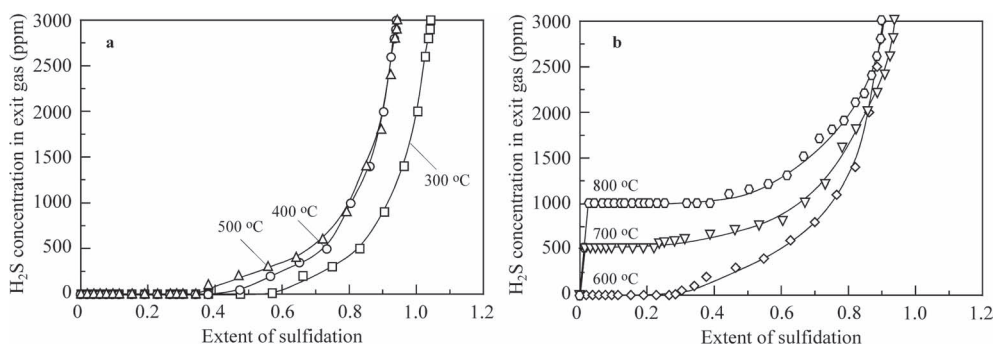

Fig. 1. Change in sulfidation behavior of limonite-reduced with temperature in 50% H_2/He.
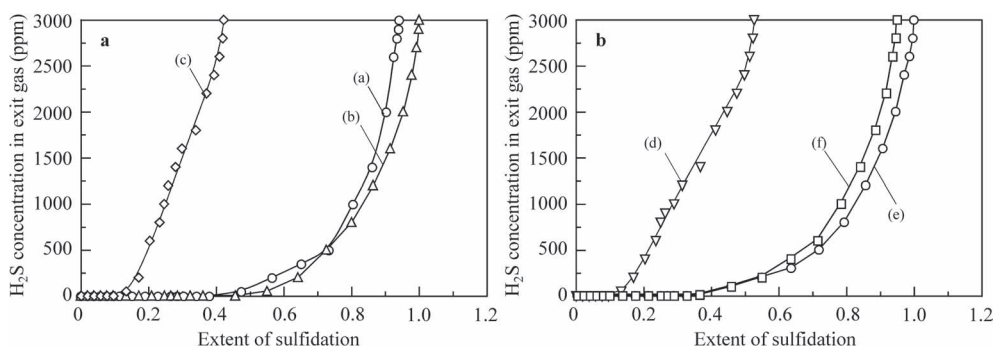

Fig. 2. Influence of coexisting gases on the relationships between the extent of sulfidation and H_2S concentraction in the exit gas at 400°C. (a) In 50% H_2/He, (b) In 50% H_2/30% CH_4/He, (c) In 50% H_2/30% CH_4/5% CO/He, (d) 50% H_2/30% CH_4/5% CO/5% CO_2/He, (e) 50% H_2/30% CH_4/5% CO/5% H_2O/He, (f) 50% H_2/30% CH_4/5% CO/5% CO_2/5% H_2O/He.

Table 2. Summaries of breakthrough and saturation point at breakthrough curves and sulfidation curves with H_2S/Fe ratio at 400°C.

Atmosphere	Breakthrough curve		Extent of sulfidation (H_2S/Fe)		
	Breakthrough point (min)	Saturation point (min)	At breakthrough point	At saturation point	At after reaction
$50\%H_2/He$	35	65	0.65	0.93	0.95
$50\%H_2/30\%CH_4/He$	32	65	0.68	1.00	1.00
$50\%H_2/30\%CH_4/5\%CO/He$	10	38	0.18	0.41	0.42
$50\%H_2/30\%CH_4/5\%CO/5\%CO_2/He$	10	42	0.18	0.51	0.53
$50\%H_2/30\%CH_4/5\%CO/5\%H_2O/He$	32	67	0.63	0.98	1.00
$50\%H_2/30\%CH_4/5\%CO/5\%CO_2/5\%H_2O/He$	28	60	0.63	0.94	0.95

fidation extent of 0.65 and 0.93, respectively (Fig. 2(a)). When 30% CH_4 was added to 50% H_2/He, the breakthrough and saturation points were observed at 32 and 65 min, corresponding to sulfidation extent of 0.68 and 1.0, respectively, as well as those in 50% H_2/He, and the presence of CH_4 did not significantly affect H_2S removal. On the other hand, the breakthrough and saturation times in 50% $H_2/30\%$ $CH_4/5\%$ CO/He drastically decreased from 35 and 65 min in 50% $H_2/30\%$ CH_4/He to 10 and 38 min, respectively. The extent of sulfidation at the breakthrough and saturation points also decreased to 0.18 and 0.4, respectively, and the two curves ((b) and (c) in Fig. 2(a)) were quite different. The H_2S removal performance drastically decreased in the presence of CO. Figure 2(b) also shows the results with 5% CO_2, 5% H_2O or both coexisted to 50% $H_2/30\%$ $CH_4/5\%$ CO/He. With 5% CO_2 added, the breakthrough point was observed at 10 min, and sulfidation curves was similar to that of 50% $H_2/30\%$ $CH_4/5\%$ CO/He. These results indicate that the presence of CO_2 did not affect H_2S removal in 50% $H_2/30\%$ $CH_4/5\%$ CO/He. On the other hand, the removal performance was improved with 5% H_2O addition, as seen in Fig. 2(b), and breakthrough and saturation points increased to 32 and 67 min from 10 and 38 min in presence 5% CO, respectively. As seen in Fig. 2(b), similar behavior was observed in 50% $H_2/30\%$ $CH_4/5\%$ CO/5% $CO_2/5\%$ H_2O/He. The order of sulfidation extent in Fig. 2 and Table 2 is 50% $H_2/30\%$ $CH_4/5\%$ CO/He < 50% $H_2/30\%$ $CH_4/5\%$ CO/5% CO_2/He < 50% $H_2/30\%$ $CH_4/5\%$ CO/5% $H_2O/$ He $\doteqdot$ 50% $H_2/30\%$ $CH_4/5\%$ CO/5% $CO_2/5\%$ $H_2O/He \doteqdot$ 50% $H_2/30\%$ CH_4/He. From these results, it was found that H_2O addition can improve the H_2S removal performance of limonite, whereas CO addition decreases the removal ability of reduced-limonite under these conditions.

3.2. Possible Mechanisms of Influence of COG Components on H_2S Removal Performance

XRD measurements of the samples recovered after reaction were carried out to investigate the difference in H_2S breakthrough curves with coexisting gases at 400°C. The results are summarized in **Table 3**. In these samples, iron always takes the form of $Fe_{1-x}S$, regardless of the gas composition used, and thus, it was difficult to clarify the influence of coexisting gases on the H_2S removal performance from the XRD results alone. Therefore, TPO of the samples were investigated in 10% O_2/He up to 950°C, as shown in **Fig. 3**. No CO and CO_2 evolution was measured

Table 3. Crystalline form of Fe after H_2S removal in different atmosphere and the amount of CO and CO_2 evolved during temperature programmed oxidation of samples after sulfidation.

Atmosphere	Iron species after H_2S removal[a]	Evolution amount (μmol/g)	
		CO	CO_2
$50\%H_2/30\%CH_4/He$	$Fe_{1-x}S$(m)	0	10
$50\%H_2/30\%CH_4/5\%CO/He$	$Fe_{1-x}S$(m)	290	1 400
$50\%H_2/30\%CH_4/5\%CO/5\%CO_2/He$	$Fe_{1-x}S$(m)	210	1 100
$50\%H_2/30\%CH_4/5\%CO/5\%H_2O/He$	$Fe_{1-x}S$(m)	40	180
$50\%H_2/30\%CH_4/5\%CO/5\%CO_2/5\%H_2O/He$	$Fe_{1-x}S$(m)	30	60

[a]XRD intensities designated by m (medium)

during TPO of the sample recovered after the 50% $H_2/30\%$ CH_4/He run. However, during TPO of the sample after the 50% $H_2/30\%$ $CH_4/5\%$ CO/He run, CO and CO_2 were evolved above approximately 300°C (Fig. 3(a)), with main and shoulder peaks for the CO and CO_2 formation rates at approximately 350 and 450°C, respectively. As similar profile was observed for sample recovered after the 50% $H_2/30\%$ $CH_4/5\%$ CO/5% CO_2/He run (Fig. 3(b)). On the other hand, the peaks of the CO and CO_2 formation rates from the samples recovered after the 50% $H_2/30\%$ $CH_4/5\%$ CO/5% H_2O/He and 50% $H_2/30\%$ $CH_4/5\%$ CO/5% $CO_2/5\%$ H_2O/He runs were considerably smaller than those for coexisting CH_4/CO and $CH_4/CO/CO_2$ (Fig. 3(c)). Table 3 summaries of the amounts of CO and CO_2 evolved during the TPO runs. The $Fe_{1-x}S$ observed in all samples after H_2S treatment was completely transformed into Fe_2O_3 after TPO. The order of the amounts of CO and CO_2 evolved during TPO is 50% $H_2/30\%$ CH_4/He < 50% $H_2/30\%$ $CH_4/5\%$ CO/5% $CO_2/5\%$ H_2O/He < 50% $H_2/30\%$ $CH_4/5\%$ CO/5% H_2O/He << 50% $H_2/30\%$ $CH_4/5\%$ CO/5% $CO_2/He \leq$ 50% $H_2/30\%$ $CH_4/5\%$ CO/He. This order was almost the inverse of that for the amount of H_2S removal.

The reaction between metallic Fe and H_2S is well known to occur according to Eqs. (1) and (2) to form pyrrhotite ($Fe_{1-x}S$) and iron sulfide (FeS), and these reactions are supported by thermodynamic calculations because the corresponding standard Gibbs free energies ($\triangle$G) at 400°C are -13 and -14 kcal/mol.
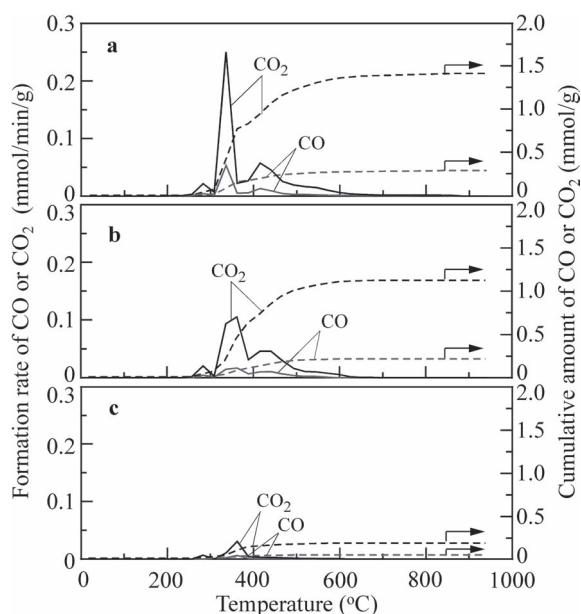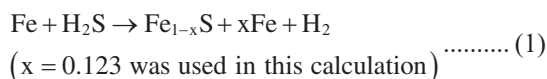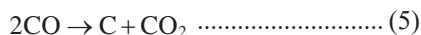
Fig. 3. Formation rate and cumulative amount of CO or CO_2 during temperature-programmed oxidation of samples after sulfidation: (a) In 50% H_2/30% CH_4/5% CO/He, (b) In 50% H_2/30% CH_4/5% CO/5% CO_2/He, (c) In 50% H_2/30% CH_4/5% CO/5% H_2O/He.

$$Fe + H_2S \rightarrow Fe_{1-x}S + xFe + H_2 \qquad \cdots\cdots (1)$$
$$\left(x = 0.123 \text{ was used in this calculation} \right)$$

$$Fe + H_2S \rightarrow FeS + H_2 \quad\cdots\cdots\cdots\cdots (2)$$

In addition, C deposition and Fe_3C formation from CH_4 occur according to Eqs. (3) and (4):

$$CH_4 \rightarrow C + 2H_2 \quad\cdots\cdots\cdots\cdots\cdots (3)$$

$$3Fe + CH_4 \rightarrow Fe_3C + 2H_2 \quad\cdots\cdots\cdots (4)$$
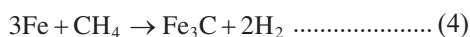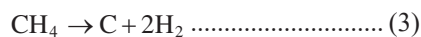
The $\triangle G_{400°C}$ values for Eqs. (3) and (4) are 3.6 and 6.0 kcal/mol, respectively, and thus, C deposition or Fe_3C formation via these is not thermodynamically favorable under these conditions. Therefore, the H_2S breakthrough curve is similar to that in 50% H_2/He. In other words, CH_4 does not affect H_2S removal by reduced-limonite under the present conditions. This is supported by the TPO results, in which no significant evolution of CO and CO_2 was observed. In the case of 5% CO addition to 50% H_2/30% CH_4/He, the H_2S removal performance decreased, as seen in Fig. 2(a). C deposition or Fe_3C formation from CO may occur according to Eqs. (5) and (6).

$$2CO \rightarrow C + CO_2 \quad\cdots\cdots\cdots\cdots (5)$$

$$3Fe + 2CO \rightarrow Fe_3C + CO_2 \quad\cdots\cdots\cdots (6)$$

$$CO + H_2 \rightarrow C + H_2O \quad\cdots\cdots\cdots\cdots (7)$$

$$3Fe + C \rightarrow Fe_3C \quad\cdots\cdots\cdots\cdots\cdots (8)$$

$$Fe_3C + 3H_2S \rightarrow 3FeS + C + 3H_2 \quad\cdots\cdots (9)$$

As the $\triangle G_{400°C}$ values for Eqs. (5) and (6) are -13 and -10 kcal/mol, respectively, these reactions are likely to be favorable under the conditions applied. The driving force for

Eq. (7) ($\triangle G_{400°C} = -9.4$ kcal/mol) is smaller than those for Eqs. (5) and (6). The $\triangle G_{400°C}$ value for Eq. (8) (2.4 kcal/mol) indicates that this reaction is also not thermodynamically favored. Although Fe_3C was not detected by XRD in the sample recovered after the run in 50% H_2/30% CH_4/5% CO/He, significant CO and CO_2 formation were observed during TPO of this sample, as seen in Fig. 3(a). Therefore, Eq. (9), which has a $\triangle G_{400°C}$ values of -45 kcal/mol, should also be considered. The decreased H_2S removal performance in the presence of CO may be caused by deposition of C derived from disproportionation reactions of CO on reduced-limonite active sites, and C deposited from Eqs. (5)–(7) and (9) will be a main factor for the decreased H_2S removal performance. The H_2S breakthrough curve in 50% H_2/30% CH_4/5% CO/5% CO_2/He was similar to that in 50% H_2/30% CH_4/5% CO/He. The Boudouard reaction ($\triangle G_{400°C} = 13$ kcal/mol), expressed as Eq. (10), is not thermodynamically favorable. In addition, if Fe_3C forms under the present conditions, Eq. (11) also does not occur ($\triangle G_{400°C} = 10$ kcal/mol). Therefore, coexisting CO_2 may not affect the removal performance of H_2S. This speculation supported by the similar amounts of CO and CO_2 evolved during TPO of the samples recovered from the 50% H_2/30% CH_4/5% CO/He and 50% H_2/30% CH_4/5% CO/5% CO_2/He runs (Table 3).

$$C + CO_2 \rightarrow 2CO \quad\cdots\cdots\cdots\cdots\cdots (10)$$

$$Fe_3C + CO_2 \rightarrow 3Fe + 2CO \quad\cdots\cdots\cdots (11)$$
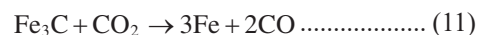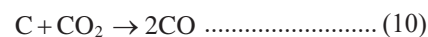
In contrast, in the cases of H_2O coexisting in the feed gases (50% H_2/30% CH_4/5% CO/5% H_2O/He or 50% H_2/30% CH_4/5% CO/5% CO_2/5% H_2O/He), the H_2S breakthrough curves showed the similar tendencies to that of 50% H_2/30% CH_4/He, and the performance of the sample with 5% CO was improved by H_2O addition. In addition, the amounts of CO and CO_2 evolved during TPO were significantly smaller than those with coexisting CO, as seen in Table 3. These results shows that C deposition is inhibited by H_2O. Although the $\triangle G_{400°C}$ values of two water-gas reactions (6.0–9.4 kcal/mol) expressed as Eqs. (12) and (13) are not thermodynamically favorable, the water-gas shift reaction of Eq. (14) ($\triangle G_{400°C} = -3.3$ kcal/mol) may occur. Although Fe_3C was not observed by XRD, the H_2S removal performance may be proceeded by the reaction shown in Eq. (9), which has a $\triangle G_{400°C}$ values (-45 kcal/mol) that is smaller than those of Eqs. (15) and (16) (3.6–7.0 kcal/mol), even if Fe_3C is formed under these present conditions. Thus it may be possible that H_2O addition prevents C deposition according to Eqs. (5)–(7) due to the water-gas shift reaction (Eq. (14)), and as a result, the H_2S removal performance is improved.
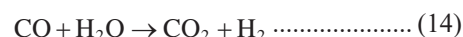
$$C + H_2O \rightarrow CO + H_2 \quad\cdots\cdots\cdots\cdots (12)$$

$$C + 2H_2O \rightarrow CO_2 + 2H_2 \quad\cdots\cdots\cdots (13)$$

$$CO + H_2O \rightarrow CO_2 + H_2 \quad\cdots\cdots\cdots (14)$$

$$Fe_3C + 2H_2O \rightarrow 3Fe + CO_2 + 2H_2 \quad\cdots\cdots (15)$$

$$Fe_3C + H_2O \rightarrow 3Fe + CO + H_2 \quad\cdots\cdots (16)$$

Figure 4 illustrated the effect of space velocity on the H_2S breakthrough curves in 50% H_2/30% CH_4/5% CO/5% CO_2/5% H_2O/He. Here, the space velocity was varied from 51 000 to 5 600 h^{-1}. When the SV decreased to 5 600 h^{-1}, H_2S was not detected in the exit gas until 120 min. The breakthrough increased more than 6-fold from 27 min at an SV of 51 000 h^{-1} to 165 min at an SV of 5 600 h^{-1}. Therefore, the breakthrough curves strongly depend on SV.

3.3. Decomposition of Ammonia in the Presence of COG Components

This section focuses on the effect of CH_4, CO, CO_2 and H_2O on limonite-catalyzed NH_3 decomposition. These runs were carried out at 850°C to simulate the utilization of COG sensible heat for NH_3 decomposition. Limonite-catalyzed N-containing species decomposition at other temperatures has been already reported at our previous reports.[10–18] **Figure 5** presents the effect of the presence of CH_4, CO, CO_2 and H_2O on NH_3 decomposition. The decomposition of NH_3 was maintained until 240 min in He, whereas N_2 conversion in 50% H_2/30% CH_4/He and 50% H_2/30% CH_4/5% CO/He dramatically decreased after 90 min. A significant amount of C deposition was found on the catalyst surface in the presence of CH_4 and/or CO. As the formation of carbonaceous materials occurred under the present conditions, the catalyst deactivation observed in 50% H_2/30% CH_4 and 50% H_2/30% CH_4/5% CO (Fig. 5) may be ascribed to C deposi-
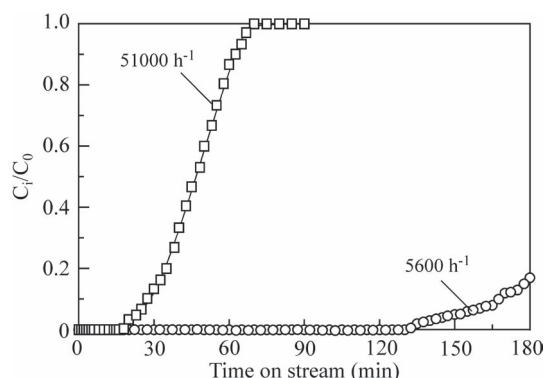

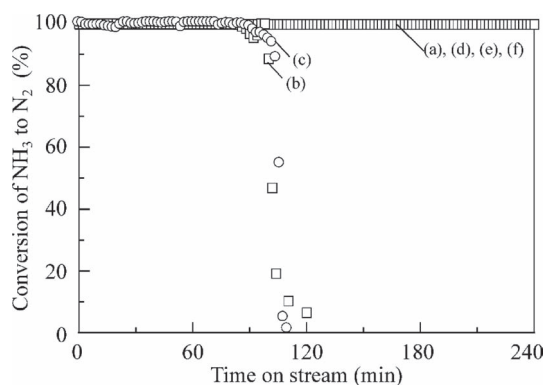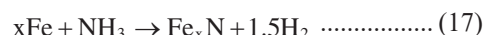**Fig. 4.** Effect of space velocity on H_2S breakthrough curves at 400°C in 50% H_2/30% CH_4/5% CO/5% CO_2/5% H_2O/He.

Fig. 5. Effect of the presence of CH_4, CO, CO_2 and H_2O on limonite-catalyzed NH_3 decomposition at 850°C. (a) In He, (b) In 50% H_2/30% CH_4/He, (c) In 50% H_2/30% CH_4/5% CO/He, (d) In 50% H_2/30% CH_4/5% CO/5% CO_2/He, (e) In 50% H_2/30% CH_4/5% CO/5% H_2O/He, (f) In 50% H_2/30% CH_4/5% CO/5% CO_2/5% H_2O/He.

tion according to the Eqs. (3) and (4), with $\triangle G_{850°C}$ values of −7.8 and −8.0 kcal/mol, respectively. These $\triangle G$ values are smaller than those of Eqs. (5), (6) and (7) ($\triangle G_{850°C}$ = 6.3, 6.1 and 6.0 kcal/mol, respectively). On the other hand, the reaction show in Eq. (8) may also occur ($\triangle G_{850°C}$ = −0.2 kcal/mol).

Figure 5 also illustrates the effects of 5% CO_2, 5% H_2O or 5% H_2O/5% CO_2 coexisting to 50% H_2/30% CH_4/5% CO on NH_3 decomposition. In 50% H_2/30% CH_4/5% CO/5% CO_2/He, 50% H_2/30% CH_4/5% CO/5% H_2O/He and 50% H_2/30% CH_4/5% CO/5% CO_2/5% H_2O/He, the NH_3 decompositions performance was maintained until 240 min, and >99% conversion of NH_3 to N_2 was observed. Moreover, no significant C deposition was found on the catalysts recovered after the experimental runs. These results show that the coexistence of CO_2, H_2O or CO_2/H_2O with 50% H_2/30% CH_4/5% CO can improve NH_3 decomposition. As mentioned above, the deactivation of limonite for NH_3 decomposition mainly occurs due to deposition of C according to Eqs. (3) and (4). From the thermodynamic calculation results, preventing C deposition in the presence of CO_2 may occur by Eqs. (10) and (11) ($\triangle G_{850°C}$ = −6.3 and −6.1 kcal/mol, respectively). On the other hand, in the case of H_2O addition to 50% H_2/30% CH_4/5% CO, $\triangle G_{850°C}$ values for Eqs. (12) and (13) are almost −6.0 and −5.8 kcal/mol, respectively, and these reactions are more favorable than Eq. (14), which has a $\triangle G_{850°C}$ value of 0.2 kcal/mol. In addition, Eqs. (15) and (16) ($\triangle G_{850°C}$ = −5.6 and −5.8 kcal/mol, respectively) are also thermodynamically favorable. Therefore, preventing C deposition and retransformation of Fe_3C into metallic Fe, as shown in Eqs. (10), (12) and (13) and Eqs. (11), (15) and (16), respectively, may be the driving force for the high NH_3 decomposition performance with 5% CO_2, 5% H_2O or 5% CO_2/5% H_2O coexisted to 50% H_2/30% CH_4/5% CO. Similar results have been reported for NH_3 decomposition by limonite in a simulated air-blown coal gasification composition (10% CO_2 or 3% H_2O coexisted in 20% CO/10% H_2).[12]

3.4. Possible Mechanisms of Influence of COG Components on NH_3 Decomposition

Figure 6 shows the XRD results for the catalysts after NH_3 decomposition in each gas composition, and these results are summarized in **Table 4**. When limonite was reduced in H_2, only α-Fe was observed (Fig. 6(a)). This signal was also observed for the catalysts recovered after the He runs, and transformation of the iron form was not observed. According to previous our studies, the catalytic decomposition of NH_3 to N_2 with reduced-limonite occurs due to the cyclic reaction via iron nitride (Fe_xN) intermediates, according to Eqs. (17) and (18).[8–14,16]

$$xFe + NH_3 \rightarrow Fe_xN + 1.5H_2 \quad \cdots\cdots\cdots\cdots (17)$$

$$Fe_xN \rightarrow xFe + 0.5N_2 \quad \cdots\cdots\cdots\cdots (18)$$

On the other hand, crystallized carbon (CC) was detected at around 32° in the samples recovered after reaction in 50% H_2/30% CH_4/He, along with peaks corresponding to α-Fe and Fe_3C. The peaks attributable to crystallized C and Fe_3C were also observed for the in catalyst after the decomposition run in 50% H_2/30% CH_4/5% CO/He. The formation
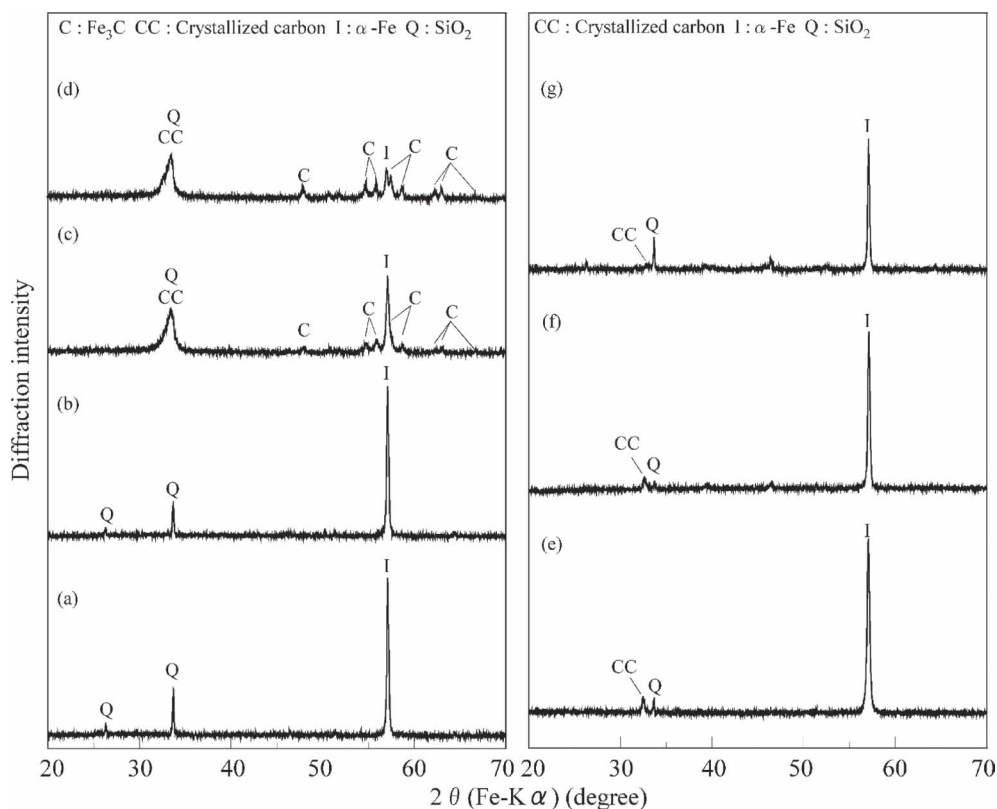
Fig. 6. XRD profiles of catalysts after NH_3 decomposition at 850°C in various atmosphere. (a) Reduced-limonite, (b) In He, (c) In 50% H_2/30% CH_4/He, (d) In 50% H_2/30% CH_4/5% CO/He, (e) In 50% H_2/30% CH_4/5% CO_2/He, (f) In 50% H_2/30% CH_4/5% CO/5% H_2O/He, (g) In 50% H_2/30% CH_4/5% CO/5% CO_2/5% H_2O/He.

Table 4. Summarize of TPO results and Fe forms after NH_3 decomposition run at different atmosphere.

NH_3 decomposition atmosphere	Iron species after NH_3 decomposition[a]	Evolution amount (μmol/g)	
		CO	CO_2
He	α-Fe (s)	n.a.[b]	n.a.[b]
50%H_2/30%CH_4/He	α-Fe(m), Fe_3C(vw), Crystallized carbon(m)	10 700	40 300
50%H_2/30%CH_4/5%CO/He	α-Fe(w), Fe_3C(w), Crystallized carbon(m)	15 300	28 700
50%H_2/30%CH_4/5%CO/5%CO_2/He	α-Fe (s)	0	350
50%H_2/30%CH_4/5%CO/5%H_2O/He	α-Fe (s)	0	40
50%H_2/30%CH_4/5%CO/5%CO_2/5%H_2O/He	α-Fe (s)	10	40

[a]XRD intensities designated by w (weak), m (medium), and s (strong), [b]Not analyzed.

of crystallized C and Fe_3C may indicate that deactivation of the catalyst occurs by Eqs. (4) and (8) ($\triangle G_{850°C} = -8.0$ and -0.2 kcal/mol, respectively), in the presence of 30% CH_4. On the other hand, no measurable Fe_3C signals were observed in the sample obtained after reaction in 50% H_2/30% CH_4/5% CO/5% CO_2/He, and the diffraction peak of crystallized C was significantly smaller than those in 50% H_2/30% CH_4/He and 50% H_2/30% CH_4/5% CO/He. In addition, the intensity of the α-Fe signal was almost that same as that of the catalyst before the reaction. Similar results were observed for the catalysts after NH_3 decomposition runs in 50% H_2/30% CH_4/5% CO/5% H_2O/He and 50% H_2/30% CH_4/5% CO/5% CO_2/5% H_2O/He. From these results, the formation of Fe_3C and crystallized C may inhibit the NH_3 decomposition performance by limonite because NH_3 conversion drastically decreased in the 50% H_2/30% CH_4/He and 50% H_2/30% CH_4/5% CO/He runs, in which Fe_3C and crystallized C were detected in the spent catalysts. Accord-

ing previous report about investigation of NH_3 decomposition by limonite and commercial Fe_3C in syngas, CO_2 or H_2O/syngas,[12] it has been suggested that the disproportionation of CO in syngas and the subsequent formation of Fe_3C are responsible for the catalyst deactivation. In addition, NH_3 decomposition performance of commercial Fe_3C is very small.[12] Therefore, the influence of Fe_3C formation on limonite-catalyzed NH_3 decomposition may be greater than that of crystallized C in this study.

Figure 7 presents the CO and CO_2 evolution profiles during TPO, and Table 4 summarizes the amounts of CO and CO_2 evolved during the TPO runs. CO and CO_2 formation started above 300°C in the sample recovered after the 50% H_2/30% CH_4/He run, with main and shoulder peaks observed in the range from 400 to 650°C (Fig. 7(a)). Similar profiles were observed for the sample obtained after the 5% CO coexisted to 50% H_2/30% CH_4/He run (Fig. 7(b)). The evolution rates of CO and CO_2 and these cumulative
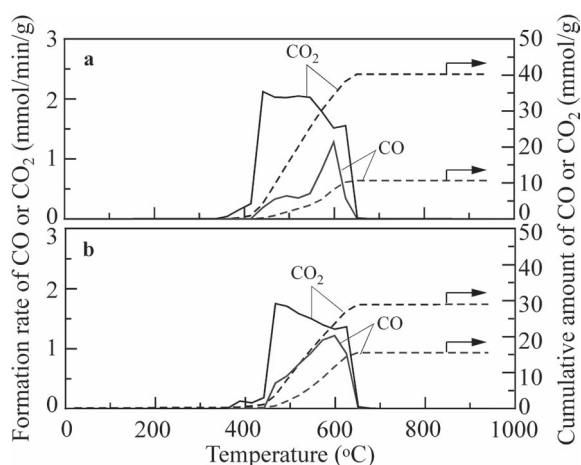
Fig. 7. Formation rate and cumulative amount of CO or CO_2 during temperature-programmed oxidation of samples after NH_3 decomposition: (a) In 50% H_2/30% CH_4/He, (b) In 50% H_2/30% CH_4/5% CO/He.

amounts were quite different with those of H_2S. This distinction may cause by the difference of deposited-C forms in H_2S removal and NH_3 decomposition runs. These forms are distinguished to amorphous-C derived from disproportionation reaction of CO in H_2S removal run and crystallized-C derived from CH_4 decomposition in NH_3 decomposition run, respectively. On the other hand, the amount of CO and CO_2 evolved during TPO of the sample recovered after in the 5% H_2O and 5% CO_2 coexisted to 50% H_2/30% CH_4/5% CO/He run were considerably smaller than those for the run in the presence of 30% CH_4 and 5% CO. These results show that C deposition is not caused by deactivation of the catalyst for NH_3 decomposition in the presence of 5% CO_2 and 5% H_2O.

4. Conclusions

The removal of 3 000 ppmv H_2S and catalytic decomposition of 1 vol% NH_3 in the presence of COG components with limonite rich in α-FeOOH has been studied in a cylindrical quartz reactor under a pressure of 0.1 MPa, temperature of 300–850°C and an SV of 51 000 h^{-1}. The principal conclusions are summarized as follows:

(1) Although the reduced-limonite shows high H_2S removal performance in 50% H_2/He, the performance decreases with increasing temperature. The XRD analyses showed that α-FeOOH-derived active α-Fe is transformed into $Fe_{1-X}S$ and FeS.

(2) In the presence of 5% CO, the H_2S removal performance at 400°C decreases considerably due to carbon deposition. In addition, 5% CO_2 addition to 50% H_2/30% CH_4/5% CO/He did not affect the H_2S removal ability of reduced-limonite.

(3) The addition of 5% H_2O to 50% H_2/30% CH_4/5% CO/He suppresses carbon formation and consequently improves the H_2S removal performance of limonite significantly.

(4) Although the limonite catalyst achieves almost complete decomposition of NH_3 in inert He at 850°C, presence of 30% CH_4 or 30% CH_4/5% CO in 50%H_2/He deactivates

limonite and causes appreciable formation of deposited carbon.

(5) When 5% CO_2, 5% H_2O or both is added to 50% H_2/30% CH_4/5% CO/He, the catalytic activity dramatically improves without carbon deposition. The NH_3 to N_2 conversion of >99% is maintained until 240 min.

(6) The XRD analyses reveal the transformation of α-FeOOH-derived active α-Fe into Fe_3C in the presence of 30% CH_4 and 30% CH_4/5% CO. On the other hand, when 5% H_2O, 5% CO_2 or 5% CO_2/5% H_2O is added to 50% H_2/30% CH_4/5% CO/He, α-Fe is the only Fe form.

REFERENCES

1) T. Aramaki: *J. Jpn. Inst. Energy*, **85** (2006), 342.
2) K. Miura, M. Kawase, H. Nakagawa, R. Ashida, T. Nakai and T. Ishikawa: *J. Chem. Eng. Jpn.*, **36** (2003), 735.
3) M. Onozaki, K. Watanabe, T. Hashimoto, H. Saegusa and Y. Katayama: *Fuel*, **85** (2006), 143.
4) L. Li, K. Morishita and T. Takarada: *J. Chem. Eng. Jpn.*, **39** (2006), 461.
5) H. Cheng, X. Lu, X. Liu, Y. Zhang and W. Ding: *J. Nat. Gas Chem.*, **18** (2009), 467.
6) N. Tsubouchi, Y. Mochizuki, Y. Ono, K. Uebo, N. Sakimoto and T. Takahashi: *Energy Fuel.*, **27** (2013), 7330.
7) Y. Mochizuki, M. Nishio, N. Tsubouchi and T. Akiyama: *Energy Fuel.*, **30** (2016), 6233.
8) Y. Ohtsuka, C. Xu, D. Kong and N. Tsubouchi: *Fuel*, **83** (2004), 685.
9) C. Xu, N. Tsubouchi, H. Hashimoto and Y. Ohtsuka: *Fuel*, **84** (2005), 1957.
10) N. Tsubouchi, H. Hashimoto and Y. Ohtsuka: *Catal. Lett.*, **105** (2005), 203.
11) N. Tsubouchi, H. Hashimoto and Y. Ohtsuka: Catalytic decomposition of ammonia in fuel gas components with inexpensive limonite at high temperatures, Advanced Gas Cleaning Technology, ed. by C. Kanaoka, H. Makino and H. Kamiya, Jugei Shobo, Tokyo, (2005), 483.
12) N. Tsubouchi, H. Hashimoto and Y. Ohtsuka: *Energy Fuel.*, **21** (2007), 3063.
13) N. Tsubouchi, H. Hashimoto and Y. Ohtsuka: *Powder Technol.*, **180** (2008), 184.
14) Y. Ohtsuka, N. Tsubouchi, T. Kikuchi and H. Hashimoto: *Powder Technol.*, **190** (2009), 340.
15) T. Matsuyama, N. Tsubouchi and Y. Ohtsuka: *J. Mol. Catal. A-Chem.*, **356** (2012), 14.
16) N. Tsubouchi, H. Hashimoto and Y. Ohtsuka: *J. Mol. Catal. A-Chem.*, **407** (2015), 75.
17) N. Tsubouchi, A. Ogawa and Y. Mochizuki: *Appl. Catal. A-Gen.*, **499** (2015), 133.
18) A. Ogawa, Y. Mochizuki and N. Tsubouchi: *ISIJ Int.*, **56** (2016), 1132.
19) Z. Meng, W.-d. Jong, R. Pal and H. M. Verkooijen: *Fuel Process. Technol.*, **91** (2010), 964.
20) S. Cheah, D. L. Carpenter and K. A. Marini-Bair: *Energy Fuel.*, **23** (2009), 5291.
21) W. Bao, Z.-y. Zhang, Z.-r. Ren, F. Li and L.-p. Chang: *Energy Fuel.*, **23** (2009), 3600.
22) B. Guo, L. Chang and K. Xie: *Ind. Eng. Chem. Res.*, **53** (2014), 8874.
23) F. Yin, J. Yu, S. Gupta. S. Wnag, D. Wang and J. Dou: *Fuel Process. Technol.*, **117** (2014), 17.
24) F. Yin, J. Yu, J. Dou, S. Gupta, B. Moghtaderi and J. Luca: *Energy Fuel.*, **28** (2014), 2481.
25) J. Yu, F. Yin S. Wnag, L. Chang and S. Gupta: *Fuel*, **108** (2013), 91.
26) Y. Fneg, J. Dou, A. Tahmasebi, J. Xu, X. Li, J. Yu and F. Yin: *Energy Fuel.*, **29** (2015), 7124.
27) K. Miura, K. Mae, T. Inoue, T. Yoshimi, H. Nakagawa and K. Hashimoto: *Ind. Eng. Chem. Res.*, **31** (1992), 415.